Ridge Concepts for the Visualization of Lagrangian Coherent Structures

Benjamin Schindler, Ronald Peikert, Raphael Fuchs and Holger Theisel

Abstract The popularity of vector field topology in the visualization community is due mainly to the topological skeleton which captures the essential information on a vector field in a set of lines or surfaces separating regions of different flow behavior. Unfortunately, vector field topology has no straightforward extension to unsteady flow, and the concept probably most closely related to the topological skeleton are the so-called Lagrangian coherent structures (LCS). LCS are material lines or material surfaces that separate regions of different flow behavior. Ideally, such structures are material lines (or surfaces) in an exact sense and at the same time maximally attracting or repelling, but practical realizations such as height ridges of the finite-time Lyapunov exponent (FTLE) fulfill these two requirements only in an approximate sense. In this paper, we quantify the deviation from exact material lines/surfaces for several FTLE-based concepts, and we propose a numerically simpler variants of FTLE ridges that has equal or better error characteristics than classical FTLE height ridges.

1 Introduction

There have been various attempts to find lines or surfaces that characterize the structures of an unsteady flow field in a similar way as topological skeletons [HH91] characterize a steady flow. The most influential approach is probably Haller's definition [Hal01] of Lagrangian coherent structures (LCS) as the *ridges* in the scalar field of finite-time Lyapunov exponents (FTLE). Numerical experiments [SLM05] have shown that these ridges coincide well with material lines (in 2D flow) or material surfaces (in 3D flow). However, this coincidence is not something that could

Benjamin Schindler, Ronald Peikert, Raphael Fuchs
ETH Zurich, e-mail: {bschindler, peikert, raphael}@inf.ethz.ch

Holger Theisel
University of Magdeburg, Germany, e-mail: theisel@isg.cs.uni-magdeburg.de

be formulated as a mathematical statement, because the FTLE contains a parameter, the integration time, and also because there are multiple definitions for a ridge. Such a statement would for example hold in the limit of infinite integration time if a steady flow is assumed. Then, the Lyapunov exponent would be constant per trajectory, and the ridges, under any reasonable definition, would be material lines. In scientific visualization, we have to deal with finite time domains, and here it turns out that FTLE ridges can deviate significantly from material lines or surfaces.

An obvious error metric for comparing different types of FTLE ridges, FTLE watersheds and related features is the flux through these lines or surfaces. The flux per unit length can be computed as the normal component of the velocity vector minus the velocity with which the feature moves in the normal direction. The latter can be estimated by tracking the feature over a small time interval.

Besides comparing different types of FTLE ridges with respect to this error metric, a second goal of this paper is to explore other FTLE-related concepts. The definition of FTLE contains a *normalization* and a *natural logarithm*. These two operations are inherited from the (infinite-time) Lyapunov exponent, where they are needed to make it independent of the starting time of a trajectory and, under the conditions of the Oseledec theorem, also independent of the trajectory. In the finite-time case these independences do not hold. Therefore, neither the logarithm nor the normalization (which both are monotone functions) are needed. By omitting the two functions, the largest eigenvalue of the (right) Cauchy-Green deformation tensor is obtained. This leads us to the study of the eigenvalues and eigenvectors of this tensor as a basis for an alternative definition of LCS lines and surfaces.

2 Related work

FTLE have been used by the fluid dynamics community for visualizing flow phenomena such as flow separation [SLM05], vortex rings [SDM06], transport barriers [LSM07], or flows generated by jellyfish [PD09]. In the visualization community, algorithms for efficient FTLE computation and subsequent visualization techniques were developed in recent years. Garth et al. [GLT*09] presented a technique for 2D flow, and later for 3D flow [GGTH07] where direct volume rendering was used to visualize the FTLE field. As an alternative to a full computation of a 3D FTLE, they proposed to compute the FTLE only on planar cross sections for gaining efficiency. Sadlo et al. [SP07] addressed the efficiency issue with a hierarchical approach where the sampling grid is refined only in the vicinity of ridges. In a later paper [SRP10], grid advection was used in order to exploit temporal coherency of time-dependent velocity data. Lipinski and Mohseni [LM10] present a method to track ridges over time to reduce the amount of FTLE computations for time-dependent data.

Besides algorithmic aspects, visualization researchers also found novel uses for FTLE. Bürger et al. computed an FTLE field for steering particle seeding in a particle-based visualization [BKKW08]. Also in terms of applications there is a

recent diversification of uses of FTLE. They have been used for visualizing the flow in the small bronchial tubes by Soni et al. [STM08] and for cell aggregation by Wiebel et al. [WCW*10].

Shadden et al. [SLM05] give an analytical and numerical analysis of the suitability of ridges of FTLE for being used as LCS. Their demonstration that FTLE ridges behave nearly as material lines is based on two non-standard ridge definitions that both have the problem that they are overdetermined (see Appendix). While they express desirable properties of ridges, the fact that practical ridges deviate from these is a motivation to study the effect of the chosen ridge definition on feature extraction from FTLE or related data.

3 Background

The *flow map* (in mathematics sometimes simply called the *flow*) of a vector field $\mathbf{u}(\mathbf{x},t)$ is the map from the point where a massless particle is seeded at time t_0 to the point where it is located at time t. The flow map is denoted by $\Phi_{t_0}^{t}(\mathbf{x})$. Formally, it is described by the following initial value problem

$$\frac{\partial}{\partial t}\Phi_{t_0}^{t}(\mathbf{x}) = \mathbf{u}(\Phi_{t_0}^{t}(\mathbf{x}),t), \qquad \Phi_{t_0}^{t_0}(\mathbf{x}) = \mathbf{x}. \tag{1}$$

Its gradient $\mathbf{F} = \nabla\Phi_{t_0}^{t}(\mathbf{x})$ leads to the *(right) Cauchy-Green deformation tensor* $\mathbf{C} = \mathbf{F}^{\top}\mathbf{F}$. With this, the *finite-time Lyapunov exponent (FTLE)* can be defined as

$$\sigma(\mathbf{x},t_0,t) = \frac{1}{|t-t_0|}\ln\left(\sqrt{\lambda_{\max}(\mathbf{C})}\right) \tag{2}$$

where $\lambda_{\max}(\mathbf{C})$ denotes the largest eigenvalue of $\mathbf{C}$.

The FTLE therefore describes the rate of separation of a pair of particles, where the maximum is taken over all spatial orientations of the pair. The FTLE can also be computed for a flow map going backward in time. In that case it describes attraction rather than repulsion.

3.1 Watersheds, height ridges, and section based ridges

Even though ridges in a 2D height field are easily recognized by the human eye, there is not a unique ridge definition. Generally, a ridge is a lower-dimensional manifold in a scalar field that generalizes the notion of a local maximum.

A natural definition of a ridge is the *watershed*. For a 2D scalar field the watershed is obtained by integrating the gradient of the field, starting at a saddle point. Intuitively, this means to walk uphill from a pass to a peak, always taking the direction of the steepest slope. In topological terms, watersheds are part of the topological

skeleton of the gradient field. This way, extension to 3D scalar fields is straightforward: They are the unstable 2D manifolds of saddle points. Sahner et al. [SWTH07] used such 2D watersheds for their concept of strain skeletons in 3D velocity fields.

Height ridges are a generalization of local maxima. A (maximum convexity) height ridge of co-dimension one is given by the points which have a zero first derivative and a negative second derivative if derivatives are taken in the direction of the minor eigenvector of the Hessian [Ebe96]. Here, the minor eigenvector refers to the eigenvector associated with the smallest *signed* eigenvalue. Often this set of points is further reduced by additional constraints in order to remove false positives [Lin98, PS08].

Section based ridges are obtained by finding local maxima in a set of parallel $n-1$-dimensional sections and connecting them [JR75]. Obviously, the orientation chosen for the sections influences the result, and reasonably good results can be expected only if the ridge is roughly orthogonal to the sections. Section based ridges have the advantage that they do not require second derivatives.

In 3D velocity fields, it can be observed that the FTLE field often has surface-like maxima, defining structures which are approximately orthogonal to the major eigenvector. Therefore, a height ridge of co-dimension one can be used to represent such structures [SP07].

4 Tensor field lines

LCS are obtained by applying any of the above ridge definitions to the FTLE field. Since the FTLE field only depends on the eigenvalues of $\mathbf{C}$, an alternative is to include also the eigenvectors of $\mathbf{C}$. The background of this is: The Cauchy-Green tensor $\mathbf{C}$ is a positive symmetric tensor, and $\mathbf{U} = \mathbf{C}^{1/2}$ is the right stretch tensor in the polar decomposition $\mathbf{F} = \mathbf{R}\mathbf{U}$, while $\mathbf{R}$ is a rotation matrix. The eigenvectors $\mathbf{N}_i$ of $\mathbf{U}$ (being also the eigenvectors of $\mathbf{C}$) are orthogonal and contain the directions of maximal and minimal stretch. The eigenvectors $\mathbf{n}_i$ of the left stretch tensor $\mathbf{V}$ (with $\mathbf{F} = \mathbf{V}\mathbf{R}$) are the vectors $\mathbf{N}_i$ after rotation, $\mathbf{n}_i = \mathbf{R}\mathbf{N}_i$ (see Fig. 1).

A *tensor field line* is obtained by integrating along the minor eigenvector of $\mathbf{C}$. The seed point for this integration can be a local FTLE maximum or another point which is assumed to lie on an LCS. Integration is stopped when a degenerate point is approached where the eigenvector direction becomes undefined. The resulting structures have the property that they are aligned with the direction of maximal stretching. Tensor field lines are included in this study as an alternative to ridges.

5 C-Ridges

Section based ridges are biased by the sectioning direction. However, this can be largely reduced by using sections that are taken orthogonal to the predicted ridge

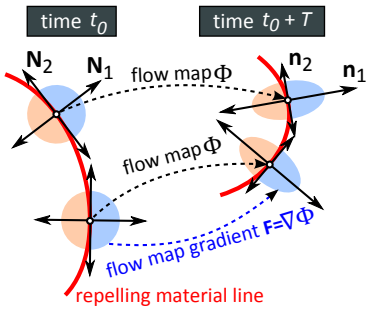

Fig. 1: Tensor field line of $\mathbf{C} = \mathbf{F}^\top\mathbf{F}$ acting as a repelling material line. When advected, its particles are mapped by Φ and their neighborhoods by $\mathbf{F}$.

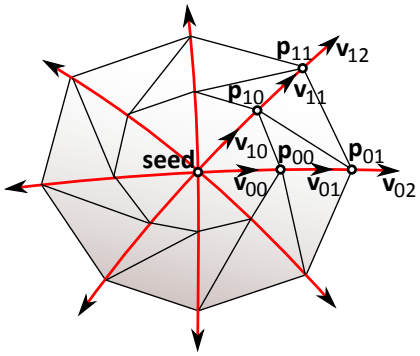

Fig. 2: Radial integration method used for $\mathbf{C}$-ridge surfaces.

direction. In our case of ridges of an FTLE field $\sigma(\mathbf{x})$, such an orthogonal direction exists, namely the major eigenvector $\mathbf{N}_1$ of $\mathbf{C}$, as was explained in Section 4. The ridge obtained this way can be expressed by

$$\mathbf{N}_1 \cdot \nabla\sigma = 0 \quad \text{and} \quad (\mathbf{H}_\sigma \cdot \mathbf{N}_1) \cdot \mathbf{N}_1 < 0 \tag{3}$$

where $\mathbf{H}_\sigma$ denotes the Hessian of σ. It differs from the height ridge only in the use of the eigenvector $\mathbf{N}_1$ which for a height ridge must be replaced by the minor eigenvector of $\mathbf{H}_\sigma$. This new type of ridge, restricted to points where $\sigma > 0$, fulfills two of the conditions of Haller's new concept of *weak LCS* (cf. [Hal10], Definition 7), while the other two (material surface, the surface itself is orthogonal to $\mathbf{N}_1$) can hold in general only in the limit $t \to \infty$. For brevity of notation, we will use the name $\mathbf{C}$-ridges for these ridges.

The $\mathbf{C}$-ridge can be extended to a surface in 3D by taking a local FTLE maximum as the seed point and a tangential plane orthogonal to the major eigenvector. In Fig. 2 we illustrate the integration approach for the $\mathbf{C}$-ridge. At the seed point the ridge normal vector is given by the major eigenvector $\mathbf{N}_1$ of $\mathbf{C}$. We choose a vector $\mathbf{v}_{00}$ normal to $\mathbf{N}_1$ and rotate this vector around $\mathbf{N}_1$ in discrete angular steps, giving vectors $\mathbf{v}_{0i}$. We denote the j^{th} integration step in the i^{th} direction as $\mathbf{v}_{ij}$ and the resulting point as $\mathbf{q}_{ij}$. At $\mathbf{q}_{ij}$ a correction step is done in the direction of the local eigenvector $\mathbf{N}_1$, maximizing the FTLE value σ. The result is denoted by $\mathbf{p}_{ij}$. The next step $\mathbf{v}_{ij+1}$ is then computed as the projection of the previous stepping direction $\mathbf{v}_{ij}$ onto the normal plane of $\mathbf{N}_1$ at the point $\mathbf{p}_{ij}$. Integration is stopped when σ drops below a given threshold.

It is worth clarifying that both height ridges and $\mathbf{C}$-ridges can be detected locally, i.e., they would not require a seed point. However, local maxima of FTLE always

lie on a ridge, and by taking (a subset of) the maxima as the seed points a subset of "important" ridges is obtained. This approach is also computationally more efficient, even though it means that duplicates must be checked for. Furthermore, it allows ridges to be tracked over time by tracking the local maximum, which is easily done by following the steepest ascent.

As a side note, the same procedure without the correction step would give the 3D analogue to the tensor field line, which has been used also for visualization [VBvP04]. However, it is well known [STS10] that a surface exactly orthogonal to the major eigenvector does not exist in general.

6 Error metric for the material line/surface property

Material lines and surfaces have the property that there is zero flux crossing the line or surface. A straightforward error metric is therefore based on the flux. When computing the flux we have to take relative velocities because the line or surface is moving. Formally, for the case of a line γ in 2D, this is

$$\int_{\gamma} (\mathbf{u}(\mathbf{x}(s,t),t) - \mathbf{c}(s,t)) \cdot \mathbf{n}(s,t) ds \tag{4}$$

where $\mathbf{x}(s,t)$ is the position of the curve point with parameter value s at time t, $\mathbf{u}(\cdot,t)$ the velocity field, $\mathbf{c}(\mathbf{s},\mathbf{t})$ is the point's velocity as given by its tracking, and $\mathbf{n}(s,t)$ is the curve normal.

For a local measure, the flux is taken per unit length (or unit area). Its computation requires computing LCS for a sequence of time steps. LCS curves (or surfaces) are tracked over time and the speed orthogonal to the LCS is derived from its motion. This speed is compared to the local velocity field, again projected onto the orthogonal space of the LCS. The difference is the *local flux*, i.e., the flux per unit length or area. Since the local flux is commensurate with a velocity, it can be *normalized* by dividing it by the local velocity magnitude. Normalized local fluxes were used by Shadden et al. [SLM05]. This error metric can be used for line-type structures in 2D domains and for line-type and surface-type structures in 3D domains.

The *tracking* of an LCS over time is done by tracking its seed point. For the majority of the above feature definitions the seed point is a local FTLE maximum, which is simply tracked by following the gradient (steepest ascent method). The remaining feature types, watersheds and tensor field separatrices, are seeded at saddle points of the FTLE field and degenerate points of the tensor field $\mathbf{C}$, respectively. These other seed points could be tracked by a critical point tracking method [TWSH02, GTS04]. For our study, we did a simple tracking by proximity.

However there is no one-to-one mapping between these seeds and the FTLE maxima where ridges are seeded. At the initial time step, the best matching watershed and tensor field separatrix have to be found manually. After each tracking step it is verified that the watershed still extends to the FTLE maximum and the sepa-

ratrix does this sufficiently close. If not, this means that a "bifurcation" event has happened. Then the tracking is stopped, and the procedure is re-initialized.

7 Results

In this section we evaluate the differently defined LCS on series of time steps of two 2D vector fields. We also use a 3D dataset from [SP07] for a qualitative comparison of height ridges and the proposed **C**-ridges.

7.1 "Double Gyre" example

The double gyre is an analytic unsteady 2D vector field which was used by Shadden et. al [SLM05] to demonstrate that saddles of vector field topology can deviate from the point of actual saddle behavior. The field is defined by

$$\begin{aligned} u(x,y,t) &= -\pi A \sin(\pi f(x,t)) \cos(\pi y) \\ v(x,y,t) &= \pi A \cos(\pi f(x,t)) \sin(\pi y) \frac{df(x,t)}{dx} \end{aligned} \tag{5}$$

where

$$f(x,t) = \varepsilon \sin(\omega t) x^2 + (1 - 2\varepsilon \sin(\omega t))\, x \tag{6}$$

and $A = 0.1, \omega = \pi/10, \varepsilon = 0.25$. First, we use long-time FTLE to reproduce the findings from Shadden et. al [SLM05]. Then, different ridge types are compared using short-time FTLE. This makes sense because the difference in flux is expected to be more pronounced when short integration times are used.

7.1.1 Results for long-time FTLE

As a first test, we measured the flux through a height ridge of an FTLE of the "double gyre" computed with integration time $T = 30$, and compared this with the findings of Shadden et al. [SLM05]. Their Fig. 8 can be roughly confirmed with our method of computing height ridges of FTLE. Also the flux through this ridge is consistent with their values. However, our height ridge computed for the same parameter values ($A = 0.1, \omega = 2\pi/10, \varepsilon = 0.1$) passes the point $x = 1.019, y = 0.9370888$ that means that the ridges disagree by about 0.0003. We computed the FTLE field using the C version of Netlib's RKF45 with relative error setting of 10^{-9} (and consistently also with 10^{-8}), and with a grid resolutions of $2 \cdot 10^{-7}$ and $2 \cdot 10^{-6}$ (see Fig.3b). We computed a flux less than 10^{-5} (five times less than computed by Shadden et al.) with either of the two resolutions. The normalized flux, as defined in Section 6 is less than 0.0002.

7.1.2 Results for short-time FTLE

The goal of [SLM05] was to investigate the sharp FTLE ridges that result from flow maps taken over a long integration time T. It is mentioned that FTLE ridges are less suitable for short times T. However, in the practice of data visualization the time domain is bounded by the available datasets, and very often it is too short to develop sharp ridges. If ridges are "soft", the different ridge definitions lead to the extraction of significantly different curves. It is one of the main purposes of this study to compare these definitions and the resulting ridge curves in terms of their geometry and their cross flux which quantifies their deviation from being material lines.

In Fig. 4, the main ridge of a short-time ($T = 3$) FTLE of the "double gyre" is shown. The height ridge (red), section-based ridge (orange), **C**-ridge (green) and tensor field line (blue) are all seeded at the local FTLE maximum near the x-axis. The FTLE watersheds (black) are seeded at a saddle point. Since there are several watersheds converging to the same local maximum, the best one in terms of cross-flux was taken for the comparison. The separatrix of the tensor field **C** (magenta) is seeded at a degenerate point. These do not converge to FTLE maxima as they are not directly related to the FTLE field. For the comparison we took the one separatrix that approaches the chosen FTLE maximum most closely.

The set of 5x5 particles in Fig. 4 shows that all curves have some particles crossing them in the time interval $(1.0, 2.0)$. Toward the bottom of the image, all feature lines except the tensor field separatrix (magenta) coincide with the two FTLE water-

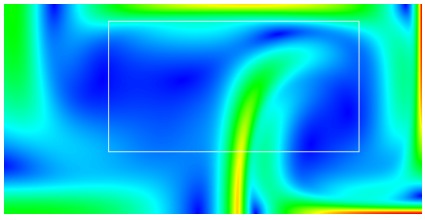

(a) FTLE at $t = 0$, integration time $T = 3$. The white rectangle marks the close-up region used in Fig. 4.

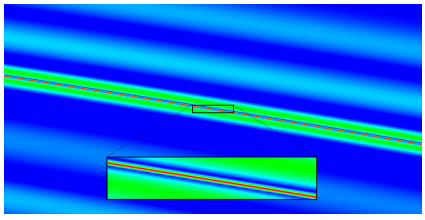

(b) FTLE with integration time $T = 30$ in the region discussed in [SLM05].

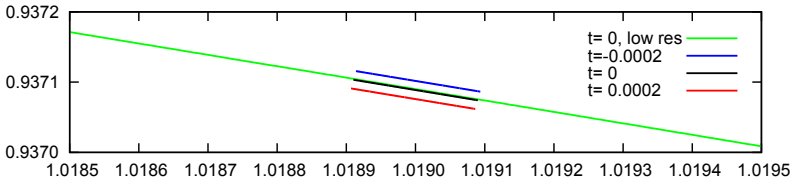

(c) Extracted height ridge on close-up region at $t = 0$ and $t = \pm 0.0002$.

Fig. 3: Short-time and long-time FTLE of the "double gyre" vector field.

sheds (black). The height ridge (red) originating at the FTLE maximum below the bottom of the image curves to the right at t=1.0 and later connects with the branch reaching to the left. In either stage the long branch of the height ridge follows closely one of the two watersheds. Also the **C**-ridge (green) closely follows it. Some of the curves are crossed by fewer particles, such as the y-section ridge (orange), the tensor field separatrix, and in particular the tensor field line (blue) which is consistent with the flux plot in Fig. 5b for the same time interval.

The evaluation result using our error metric is shown in Fig. 5 where normalized fluxes are plotted for the various types of ridge curves. In Fig. 5(a) fluxes are measured at the lower end of the ridge. Since this ridge is quite pronounced here, most curves nearly coincide. The exception is the tensor field separatrix which does not run on top of the ridge. In Fig. 5(b) where the ridge starts to fall off, it turns out that height ridges, watersheds and **C**-ridges behave similarly throughout the time domain $t = 0, \cdots, 10$.

7.2 Square cylinder example

This vector field is a transient 3D simulation of the flow about a square cylinder (or cuboid) done with Ansys' finite-volume solver CFX. The cuboid vertically extends only to one half of the computational domain, therefore the fluid (water) can flow over the top and instead of a classical von Kármán vortex street a chain of more three-dimensionally shaped vortices appears as can be seen in Fig. 6a where vortices are visualized by a λ_2 isosurface.

We use the full 3D version of the data set for a qualitative analysis. We implemented the tensor field surface as discussed in Section 5. Fig. 6b shows that it is consistent with the FTLE color-mapped on the slice. For the quantitative analysis we use this 2D slice on the half height of the cuboid. The reason is that not all of the feature lines have a well-defined 3D analogue. We cropped the slice to a rectangle of physical size 0.18 by 0.06. Only ridges passing through the seed point as indi-

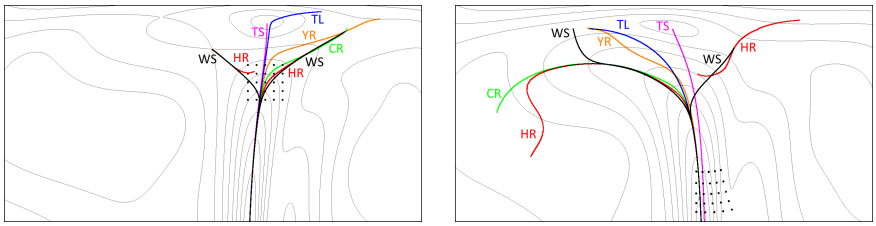

(a) Time t=1.0 (b) Time t=2.0

Fig. 4: Close-up of the "double gyre" with advected particles and the tracked feature lines: height ridges (HR), FTLE watersheds (WS), y-section ridge (YR), **C**-ridge (CR), tensor field line (TL), tensor field separatrix (TS).

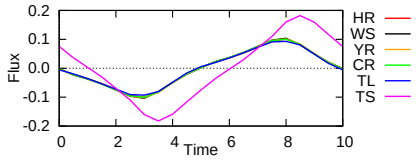

(a) Fluxes through feature lines at $y = 0.2$. (Integration time $T = 3$).

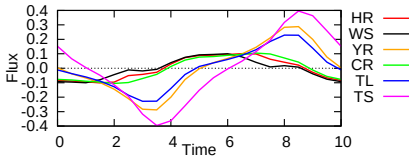

(b) Fluxes through feature lines at $y = 0.6$. (Integration time $T = 3$).

Fig. 5: Fluxes per unit length measured for the various feature lines over the full periodic time range $t = 0, \cdots, 10$ of the "double gyre" field. FTLE ridges: height ridges (HR), $y = const$ section ridges (YR), **C**-ridges (CR), watersheds (WS). Field lines of **C**: seeded at FTLE max (TL), at degenerate point (TS). Integration time used for computing C and FTLE was $T = 3$.

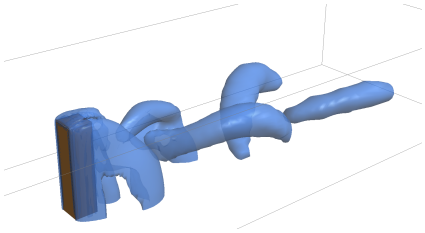

(a) Vortices (isosurfaces of λ_2).

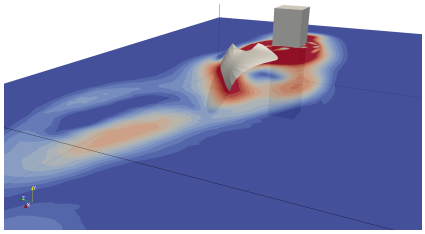

(b) **C**-ridge surface and FTLE in a slice at half height of the cylinder.

Fig. 6: Flow about a square cylinder.

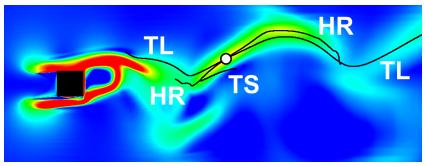

(a) Time $t = 0.13$

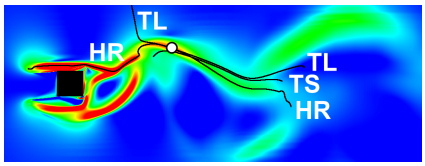

(b) Time $t = 0.14$

Fig. 7: Height ridge (HR) passing the selected local FTLE maximum (circled), tensor field line (TL) seeded at the same point, tensor field separatrix (TS) seeded at the nearest degenerate point.

cated in Fig. 7 are shown. Since the features extend mostly along the x-axis, we also added ridges based on constant x sections to the comparison. The results are plotted in Fig. 8, where we selected time steps $t = 0.13$ and $t = 0.14$ and manually picked as the seed point one of the FTLE maxima.

Similar observations as in the first example can be made here. Through all structures there is non-negligible flux. The three types of ridges give very similar results with the **C**-ridge being slightly but consistently better than the other two. The ten-

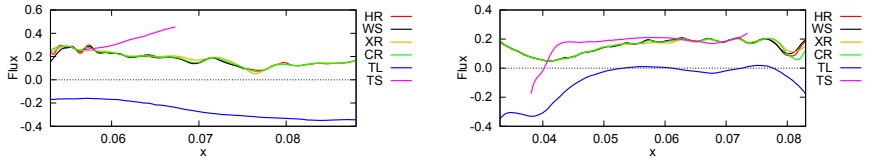

(a) Flux per unit length through feature lines, $t = 0.13$.

(b) Flux per unit length through feature lines, $t = 0.14$.

Fig. 8: Error of feature lines at selected time steps in the square cylinder example. HR: height ridge, WS: watershed, XR: $x = const$ section ridge, CR: **C**-ridge, TL: tensor field line, TS: tensor field separatrix.

sor field lines which geometrically deviates from the ridges has similar repulsion strength, but the cross-flux differs for some of the time steps quite significantly, e.g. at $t = 0.14$ there is almost no flux. The time steps $t = 0.13$ and $t = 0.14$ are shown in Fig. 7.

Summarizing the evaluation of both examples, we observe that both tensor field lines and FTLE watersheds can drift away at some point from an FTLE ridge. This is because these methods are based on integration and lack a local correction toward a maximum. With the proposed error metric, tensor field lines cannot be qualified as better or worse than FTLE ridges. We included ridges based on axis-aligned sections only for the purpose of comparison. Their simple definition and the fact that the FTLE structures happen to be roughly oriented in axes directions makes them useful as a reference.

Section based ridges with sections taken perpendicular to the minor eigenvector of **C** are, however, a valid alternative. Not only can **C**-ridges be computed with just first derivatives of FTLE (which is sufficient for iteratively finding local maxima) but also the directional information contained in **C** is exploited, which is missing in the FTLE field and therefore in its height ridges. In all cases where watersheds and height ridges are in good accordance, the **C**-ridge was found to be also consistent with them.

7.3 Francis Turbine example

This vector field is an unsteady CFD simulation of an entire Francis turbine. High FTLE values can be found at the lower end of the draft tube where it branches in two parts. This region of interest was already used by Sadlo et al. [SP07] to compute height ridges with an optimized method. Here, we compare height ridges and **C**-ridges in terms of mesh quality. By using the following brute-force method, we make sure that mesh quality is not influenced by any optimization technique.

On a regular grid the flow map Φ is computed and from this the gradient **F**, the Cauchy-Green tensor **C**, the FTLE σ as well as its gradient and Hessian $\mathbf{H}_\sigma$. All

derivatives are computed by convolving with derivatives of Gaussian. Depending on the choice of height ridges or **C**-ridges, the major eigenvector of $\mathbf{H}_\sigma$ or **C** is computed on all grid nodes. Then, in a loop over the cells, the Marching Ridges algorithm [FP01] is applied. This consists of using principal component analysis to convert the eigenvectors into a consistently oriented vector field **e** and then computing the zero-level isosurface of $\mathbf{e} \cdot \nabla\sigma$. The Asymptotic Decider [NH91] method is used for the disambiguation. Finally, all triangles are trimmed at the isoline $\sigma = \sigma_{min}$ for removing parts below a threshold and at the isoline $(\mathbf{H}_\sigma \mathbf{e}) \cdot \mathbf{e} = 0$ to remove non-ridge parts ("connector surfaces" [Dam99]).

Fig. 9 shows that while the two types of FTLE ridges generally coincide, the height ridge is much noisier. The standard deviation of the Gaussian kernel is a parameter that affects the smoothness of the ridges. This effect of the scale on ridges can be studied in a scale-space setting [KSSW09,FSP11]. In our study, several fixed values were used (for Fig. 9 twice the flow map resolution), and the quality difference between the two types of ridges was found to be consistent. It can therefore be attributed to the fact that second derivatives of σ are needed in the **C**-ridge only for the trimming of triangles, but not for the ridge extraction itself.

8 Conclusion

By computing the flux through various types of ridges of FTLE fields, we confirmed the findings made in [SLM05] and we demonstrated that for shorter integration times the normalized flux can be 0.1 or more.

We introduced the **C**-ridge and showed that it is a good alternative to FTLE height ridges, because it proved to be slightly better quite consistently. The main advantage of the **C**-ridge is that it only uses eigenvectors of **C**, i.e. information that is basically available when the FTLE field is computed, and first derivatives of FTLE for the

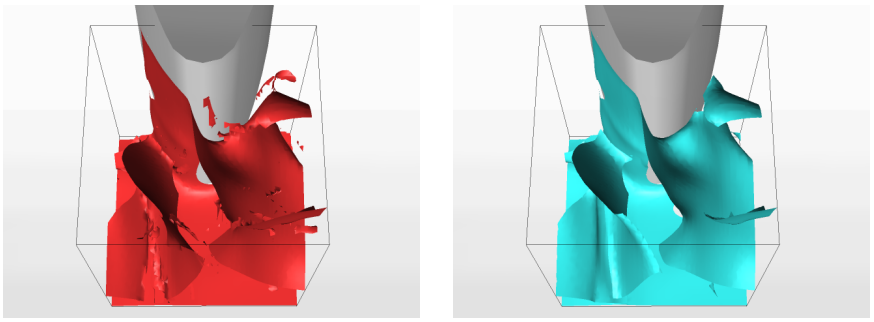

(a) (b)

Fig. 9: Comparison of height ridge (a) and **C**-ridge (b) in Francis turbine data, both extracted with Marching Ridges method.

maximum search. Height ridges require second derivatives which is numerically problematic since the FTLE field already required a numerical differentiation.

Acknowledgments

We thank Youcef Ait-Bouziad and Filip Sadlo for the simulation of the flow about a cuboid, and Andritz Hydro for the Francis turbine dataset. This work was partially funded by the Swiss National Science Foundation under grant 200021_127022. The project SemSeg acknowledges the financial support of the Future and Emerging Technologies (FET) programme within the Seventh Framework Programme for Research of the European Commission, under FET-Open grant number 226042.

References

[BKKW08] BÜRGER K., KONDRATIEVA P., KRÜGER J., WESTERMANN R.: Importance-driven particle techniques for flow visualization. In *Proceedings of IEEE VGTC Pacific Visualization Symposium 2008* (2008), pp. 71–78.

[Dam99] DAMON J.: Properties of Ridges and Cores for Two-Dimensional Images. *J. Math. Imaging Vis. 10*, 2 (1999), 163–174.

[Ebe96] EBERLY D.: *Ridges in Image and Data Analysis*. Computational Imaging and Vision. Kluwer Academic Publishers, 1996.

[FP01] FURST J. D., PIZER S. M.: Marching ridges. In *Proc. IASTED Int'l Conf. Signal and Image Processing* (2001), pp. 22–26.

[FSP11] FUCHS R., SCHINDLER B., PEIKERT R.: Scale-Space Approaches to FTLE Ridges. In *Topological Methods in Data Analysis and Visualization II (submitted)* (2011), Peikert R., Hauser H., Carr H., Fuchs R., (Eds.), Springer.

[GGTH07] GARTH C., GERHARDT F., TRICOCHE X., HAGEN H.: Efficient computation and visualization of coherent structures in fluid flow applications. *IEEE Transactions on Visualization and Computer Graphics 13*, 6 (Sep 2007), 1464–1471.

[GLT*09] GARTH C., LI G.-S., TRICOCHE X., HANSEN C. D., HAGEN H.: Visualization of coherent structures in transient 2d flows. In *Topology-Based Methods in Visualization II* (2009), Hege, Polthier, Scheuermann, (Eds.), A K Peters.

[GTS04] GARTH C., TRICOCHE X., SCHEUERMANN G.: Tracking of vector field singularities in unstructured 3d time-dependent datasets. In *Proc. of IEEE Visualization 2004* (2004), pp. 329–336.

[Hal01] HALLER G.: Distinguished material surfaces and coherent structures in three-dimensional fluid flows. *Physica D 149* (2001), 248–277.

[Hal10] HALLER G.: A variational theory of hyperbolic Lagrangian Coherent Structures. *Physica D: Nonlinear Phenomena 240*, 7 (2010), 574–598.

[HH91] HELMAN J., HESSELINK L.: Visualizing vector field topology in fluid flows. *IEEE Computer Graphics and Applications 11* (May 1991), 36–46.

[JR75] JOHNSTON E., ROSENFELD A.: Digital detection of pits, peaks, ridges, and ravines. *IEEE Transactions on Systems, Man, and Cybernetics 5* (July 1975), 472–480.

[KSSW09] KINDLMANN G. L., SAN JOSE ESTEPAR R., SMITH S. M., WESTIN C.-F.: Sampling and visualizing creases with scale-space particles. *IEEE Trans. Visualization and Computer Graphics 15*, 6 (Nov/Dec 2009), 1415–1424.

[Lin98] LINDEBERG T.: Edge detection and ridge detection with automatic scale selection. *International Journal of Computer Vision 30*, 2 (1998), 117–154.

[LM10] LIPINSKI D., MOHSENI K.: A ridge tracking algorithm and error estimate for efficient computation of lagrangian coherent structures. *Chaos 20*, 1 (2010), 017504.1–017504.9.

[LSM07] LEKIEN F., SHADDEN S. C., MARSDEN J. E.: Lagrangian coherent structures in n-dimensional systems. *Journal of Mathematical Physics 48*, 6 (2007), 065404.

[NH91] NIELSON G., HAMANN B.: The asymptotic decider: Resolving the ambiguity in marching cubes. In *Proc. of IEEE Visualization '91* (1991), pp. 83–91.

[PD09] PENG J., DABIRI J. O.: Transport of inertial particles by Lagrangian coherent structures: application to predator-prey interaction in jellyfish feeding. *J. Fluid Mech. 623* (2009), 75–84.

[PS08] PEIKERT R., SADLO F.: Height Ridge Computation and Filtering for Visualization. In *Proceedings of Pacific Vis 2008* (March 2008), Fujishiro I., Li H., Ma K.-L., (Eds.), pp. 119–126.

[SDM06] SHADDEN S. C., DABIRI J. O., MARSDEN J. E.: Lagrangian analysis of fluid transport in empirical vortex ring flows. *Physics of Fluids 18*, 4 (2006), 047105.

[SLM05] SHADDEN S., LEKIEN F., MARSDEN J.: Definition and properties of Lagrangian coherent structures from finite-time Lyapunov exponents in two-dimensional aperiodic flows. *Physica D Nonlinear Phenomena 212* (Dec. 2005), 271–304.

[SP07] SADLO F., PEIKERT R.: Efficient Visualization of Lagrangian Coherent Structures by Filtered AMR Ridge Extraction. *IEEE Transactions on Visualization and Computer Graphics 13*, 6 (Nov 2007), 1456–1463.

[SRP10] SADLO F., RIGAZZI A., PEIKERT R.: Time-Dependent Visualization of Lagrangian Coherent Structures by Grid Advection. In *Topological Data Analysis and Visualization: Theory, Algorithms and Applications*, Pascucci, Tricoche, Hagen, Tierny, (Eds.). Springer, 2010, pp. 151–166.

[STM08] SONI B., THOMPSON D., MACHIRAJU R.: Visualizing particle/flow structure interactions in the small bronchial tubes. *IEEE Transactions on Visualization and Computer Graphics 14*, 6 (2008), 1412–1427.

[STS10] SCHULTZ T., THEISEL H., SEIDEL H.-P.: Crease Surfaces: From Theory to Extraction and Application to Diffusion Tensor MRI. *IEEE Transactions on Visualization and Computer Graphics 16* (2010), 109–119.

[SWTH07] SAHNER J., WEINKAUF T., TEUBER N., HEGE H.-C.: Vortex and Strain Skeletons in Eulerian and Lagrangian Frames. *IEEE Transactions on Visualization and Computer Graphics 13*, 5 (Sep 2007), 980–990.

[TWSH02] TRICOCHE X., WISCHGOLL T., SCHEUERMANN G., HAGEN H.: Topology tracking for the visualization of time-dependent two-dimensional flows. *Computers & Graphics 26*, 2 (2002), 249–257.

[VBvP04] VILANOVA A., BERENSCHOT G., VAN PUL C.: DTI Visualization with Stream Surfaces and Evenly-Spaced Volume Seeding. In *Proc. VisSym* (2004), Deussen O., Hansen C., Keim D., Saupe D., (Eds.), pp. 173–182.

[WCW*10] WIEBEL A., CHAN R., WOLF C., ROBITZKI A., STEVENS A., SCHEUERMANN G.: Topological Flow Structures in a Mathematical Model for Rotation-Mediated Cell Aggregation. In *Topological Data Analysis and Visualization: Theory, Algorithms and Applications*, Pascucci, Tricoche, Hagen, Tierny, (Eds.). Springer, 2010, pp. 193–204.

Appendix

In ref. [SLM05] two alternative ridge definitions are used, both of which are overdetermined and can therefore not be strictly fulfilled in general. In definition 2.2 of the

second-derivative ridge, condition SR1 says that the curve must everywhere be tangent to the gradient of the FTLE field, i.e., it must be a *slope line* of σ. Together with an initial condition this fully specifies the curve, e.g., a *watershed* of σ if a saddle point is taken as the seed point. Condition SR2 also prescribes the tangent direction of the ridge curve at each of its points, this time as the eigenvector of the Hessian of σ corresponding to the larger (signed) eigenvalue. An additional constraint is that the other eigenvalue must be negative. Again, condition SR2 specifies the curve up to a seed point. For practical ridges this means that at least one of these conditions holds only approximately. Condition SR2 can be transformed into the standard definition of the (maximum convexity) *height ridge* [Ebe96] by replacing the tangent direction of the ridge by $\nabla\sigma$. Height ridges, if they are sufficiently "sharp", fulfill SR1 in an approximate sense. A relaxed version of SR1 can be used to post-filter the set of computed height ridges, e.g. by allowing for a certain maximum angle between the ridge and $\nabla\sigma$ [PS08]. Definition 2.1 of the *curvature ridge* is overdetermined in the same way as definition 2.2, therefore both definitions must necessarily be relaxed to become practically usable as, for example, watersheds, height ridges or surface creases.